Rev.Adv.Mater.Sci. 24(2010) 1-9

# COMPARATIVE MATERIAL STUDY BETWEEN PZT CERAMIC AND NEWER CRYSTALLINE PMN-PT AND PZN-PT MATERIALS FOR COMPOSITE BIMORPH ACTUATORS

**Ioan Alexandru Ivan[1], Micky Rakotondrabe[1], Joël Agnus[1], Roger Bourquin[2], Nicolas Chaillet[1], Philippe Lutz[1], Jean-Claude Poncot[3], Roland Duffait[3] and Olivier Bauer[3]**

[1]Automatic Control and Micro-Mechatronic Systems (AS2M) Department, FEMTO-ST Institute, CNRS UMR 6174, UFC, ENSMM, UTBM, 24, rue Alain Savary, 25000 Besancon, France
[2]Time Frequency (TF) Department, FEMTO-ST Institute, 26, Chemin de l'Epitaphe, 25000 Besancon, France
[3]Technology Development Department (DDT) of Pierre-Vernier Institute (IPV), 24 rue Alain Savary, 25000, France

*Received: July 17, 2009*

**Abstract.** The advent of commercially available giant piezoelectric coefficient monocrystalline materials such as PMN-PT (lead magnesium niobate - lead titanate) or PZN-PT (lead zinc niobate - lead titanate) broadens the gate for silicon-integrated applications (PiezoMEMS). Becoming more compatible with microtechnology batch processes, further advances are expected in terms of miniaturization, optimization, functionality or integration with electronics, all while reducing manufacturing costs. Subsequently, operating voltage will be lower and devices response time will improve dramatically. The paper compiles a base knowledge for composite bimorph actuators in line with a bottom-up approach for further more complex piezoelectric device designs such as "microrobots-on-chip". Material properties and constitutive equations of piezoelectric bimorph cantilevers are initially overviewed. Analytical and finite elements modeling (FEM) are afterwards performed on two designs: classical PZT on copper cantilevers and innovative PMN-PT and PZN-PT on silicon. Comparative results clearly report quantitative improvement of PMN-PT on Si design in terms of tip displacement and blocking force.



## 1. INTRODUCTION

Piezoelectric actuators started being commercially designed and manufactured about four decades ago, spreading our days into an ever increasing spectrum of applications related to positioning and motion control. An exhaustive list would be very long; hence we can only mention the actual "trends" in the above areas:

· Precision Mechanics:
  *Stimulation or active cancellation of vibrations;*
  *Precision tool adjustment;*
  *Micro and nanopositioning stages;*
  *Rotary and linear piezo drives (Inch-Worm, Stick-Slip, Ultrasonic Motors);*
  *Microgrippers;*
  *Microvalves.*
· Robotics:
  *Micro/nanomanipulators;*
  *Mobile microrobots.*
· Microtechnology:
  *Microlithography;*
  *Wafer and mask alignment;*

Corresponding author: Ioan Alexandru Ivan, e-mail: alex.ivan@femto-st.fr

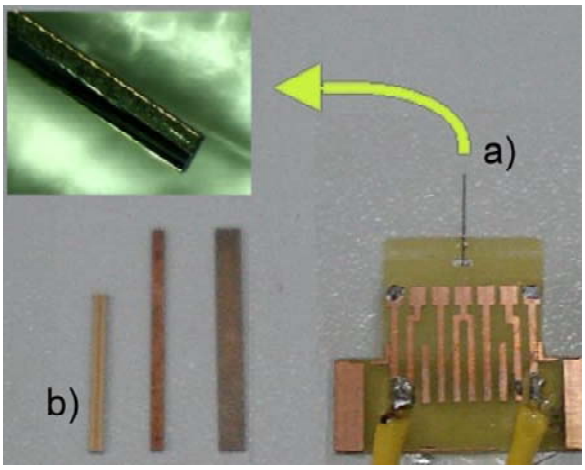


**Fig. 1.** Miniaturised PZT piezo cantilever (a) of 6.0x0.04x0.2 mm developed at IPV/DDT. Comparison with regular-size actuators (b).

*Inspection system, e.g. profilometers.*

· Optics, Nanometrology:

*Image stabilization;*
*Auto focus systems;*
*Scanning mirrors;*
*Adaptive optics;*
*Interferometry;*
*Scanning microscopy (AFM, STM etc.);*
*Optic fiber alignment.*

· Bio-Medical:

*Living cell and gene manipulation;*
*Microdispensers;*
*Micro- to pico-liter pumps.*

Piezoelectric devices can perform actuation and micropositioning tasks with resolutions from micrometers down to sub-nanometer scale. Blocking force can range from several thousand Newtons (stacked actuators) to less than microNewtons (AFM, piezocantilever, etc.). In static operation the power consumption is extremely small while in dynamic operation, settling time can be far under a millisecond.

PiezoMEMS actuators started to emerge for several years, usually made of deposited films of AlN, $BaTiO_3$ or PZT ($Pb[Zr,Ti]O_3$). New single-cristal materials such as PMN-PT and PZN-PT provide higher piezoelectric properties, energy density and electromechanical coupling factors. Several applications were reported such as in [1,2] but they are not yet silicon-integrated.

In this trend for functional miniaturization, IPV/DDT department recently developed a new technique for molecular-level bonding and lapping of piezoelectric layers on silicon wafer. Adhesives are eliminated and interface mechanical strength increased. First attempts on composite bimorph cantilevers (Fig. 1) are promising. Dimensions were reduced from 15.0 x 2.0 x 0.4 mm (central-bottom in image) to only 6.0 x 0.04 x 0.2 mm. IPV is currently developing a new series of miniaturized PMN-PT micro-actuators on silicon.

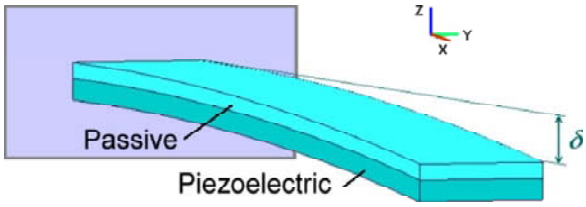


**Fig. 2.** Bending piezo-cantilever and its corresponding axis system.

This paper presents a comparative performance analysis of piezocantilevers based on PMNPT, PZNPT and PZT materials. The analysis deals with the blocking-force and the displacement at the tip of the cantilever according to its sizes and to the applied voltage. Simulation of theoretical formulations is compared with Finite Elements Method (FEM) results in order to obtain and discuss their performances.

The paper is organized as follows. Section 2 reminds PMN-PT and PZT materials for possible bending actuators. Then, the constituent equations of a bending piezoactuator (piezocantilever) are given in Section 3. Section 4 describes the comparative results of PMN-PT and PZT based piezocantilevers. Finally, section-V is dedicated to some remarks.

## 2. PIEZOELECTRIC MATERIALS FOR BENDING CANTILEVERS

Uniaxial PZT sintered ceramics are well known in static or resonant sensors and actuator applications. PMN-PT crystals started also being employed but especially into ultrasonic transducers. Their potential for actuator designs is yet to be fully revealed.

A comparative overview between classical PZT and newer PMN-PT piezoelectric materials is to be presented for composite bimorph actuators (sometimes referred as unimorphs in literature). We will consider the classical rectangular blocked-free bender design where the piezoelectric plate (layer) is bonded or deposited on a passive substrate. The axis directions are given in Fig. 2.

These types of devices work in transverse mode, for this purpose transverse $d_{31}$ piezoelectric coefficient is of most importance.

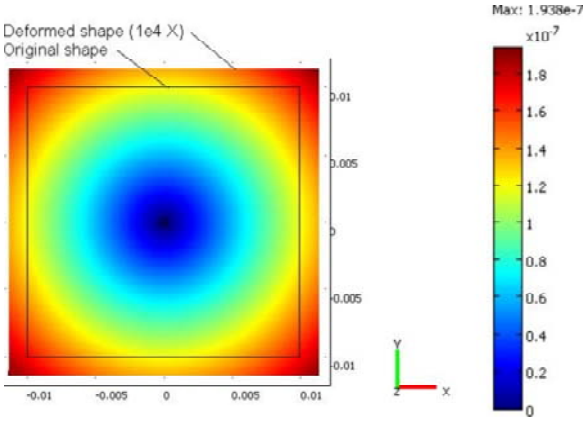


**Fig. 3.** FEM of PZT-5H plate stretching: original (20x20x0.2 mm) and deformed ($10^4$ times) shape. Coefficients given by Morgan Electroceramics.

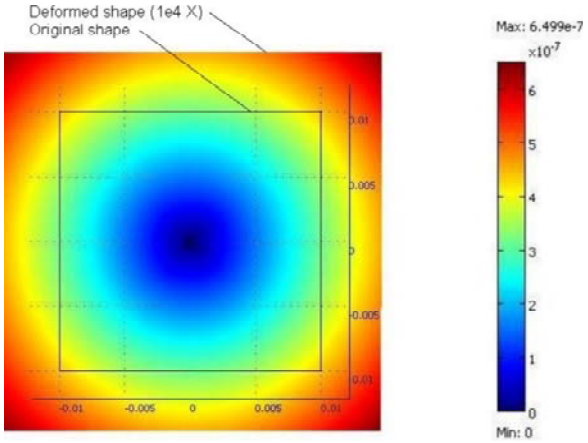


**Fig. 4.** FEM of PMN-30PT plate poled along [001]: original and deformed shape ($10^4$ times). Coefficients taken from [5].

**Table 1.** Overview of typical PZT ceramic properties from several manufacturers (PI Ceramic, Morgan, APC etc.).

| Material | $s^E_{11}$1/TPa | $s^E_{33}$1/TPa | $d_{31}$pm/V | $d_{33}$pm/V | $\varepsilon^T_{33}1/\varepsilon_0$ | $k_{31}$ |
|---|---|---|---|---|---|---|
| Soft PZTs | 15-17 | 19-22 | -140 to -280 | 300 to 600 | 1350 to 4200 | 0.28 to 0.48 |
| Hard PZTs | 8-13 | 8-14 | -42 to -140 | 130 to 475 | 950 to 1650 | 0.16 to 0.35 |

## 2.1. PZT material

About five decades ago it was discovered that the $Pb[Zr_XTi_1\text{-}X]O_3$ system, abbreviated PZT, possesses exploitable ferroelectric properties for compositions around $x$ =0.52 where the symmetry is rather complex, i.e. a mixt of tetragonal, rhomboedral and monoclinic [3]. Application of external field in PZT isotropic ceramics (temperature above 100 °C) leads to domain alignment and important piezoelectric properties. Symmetry of poled PZT is uniaxial, the matrix of coefficients being similar to that of a 6mm class, represented by a number of 13 independent constants.

Depending on doping, PZT materials are classified as soft or hard. Soft PZT is mostly used for actuators and sensors while hard PZT is employed for ultrasonic applications, exhibiting less mechanical losses but smaller piezoelectric coefficients. There are many types of commercially available PZT ceramics, and usually manufacturers classify their own products. Ranges of several elastic, piezoelectric and dielectric coefficients as well as the transverse coupling factor $k_{31}$ (square root of ratio between converted mechanical energy and input electrical energy for XZ directions) are depicted in the Table 1.

We will employ in simulations the soft PZT-5H material that is well known for its highest piezoelectric properties.

More recently, technological advances allowed deposition of thin films of PZT. Several methods became possible: chemical vapor deposition, sol-gel [4], screen-printing, RF magnetron sputtering or hydrothermal deposition. Very recently, epitaxial directly growth on silicon was also achieved. However, as a rule PZT single or multilayer thin films significantly possess reduced piezoelectric properties relative to that of regular ceramics.

## 2.2. PMN-PT and PZN-PT materials and manufacturers

In the recent years there has been an increasing interest in growing and characterizing of $x$Pb$(Mg_{1/3}Nb_{2/3})O_3$–(1-$x$)$PbTiO_3$ (PMN–PT) [5-9] and of $x$Pb$(Zn_{1/3}Nb_{2/3})O_3$–(1-$x$)$PbTiO_3$ (PZN–PT) [10-12] solid solutions. Initially used as ceramic, they can be actually grown into single crystals by modified Bridgman or solid-state single crystal growth methods [13].

These materials exhibit ultra-high piezoelectric properties for compositions near morphotropic phase

**Table 2.** Overview of PMN-PT and PZN-PT properties for concentrations around morphotropic phase boundary.

| Material, poling dir. | $s^E_{11}$ 1/TPa | $s^E_{33}$ 1/TPa | $d_{31}$ pm/V | $d_{32}$ pm/V | $d_{33}$ pm/V | $d_{15}$ pm/V |
|---|---|---|---|---|---|---|
| PMN-PT [001] | 50-70 | 40-120 | -800 to -1500 | $=d_{31}$ | 1500 to 3000 | < 160 |
| PMN-PT [011] | ~18 | 50-90 | $\approx$-1/3$d_{32}$ | -1200 to -1900 | 400 to 1000 | 1100 to 2500 |
| PMN-PT [111] | N/A | N/A | >-250 | >-250 | <450 | 3000 to 7000 |
| PZN-PT [001] | 80-90 | 110-145 | -950 to -1600 | $=d_{31}$ | 2000 to 2900 | 140-180 |
| PZN-PT [011] | ~68 | ~60 | $\approx$-1/3$d_{32}$ | ~-1460 | ~1150 | ~1800 |

boundary which is located at $x$ = 65% for PMN-PT and $x$ = 91.5% for PZNPT. Finally, electrostrictive properties are also high [14].

Initial spontaneous polarization directions are symmetric, external poling is therefore required to "privilege" certain directions into engineered domains appropriate for maximum longitudinal, transverse or shear strains. Various sets of piezoelectric elastic and dielectric matrices are provided in literature for different concentrations, cuts and poling directions.

Near morphotropic phase boundary these materials are in a rhomboedral symmetry of 3 mm class. Crystalline axes are referred in a pseudo-cubic system. Spontaneous polarization directions of each domain unit cell are along one of the eight cubic directions <111>. External polarization along [001] axis produces a tetragonal 4 mm symmetry structure, privileging longitudinal ($d_{33}$) and transverse ($d_{31}$=$d_{32}$) extension.

Cutting and poling along [011] will lead to macroscopic orthorhombic 2 mm symmetry where crystal is highest sensitive in a single transverse direction, showing a huge $d_{32}$ constant (negative value). This type of symmetry is particularly interesting because, unlike PZT ceramics, $d_{31}$ presents a positive sign (see Table 2), which theoretically allows an increased strain along axis-2 (Y-direction).

Very high longitudinal or transverse shear ($d_{15}$, $d_{24}$) may be obtained if poling in [111] directions (3 m symmetry) but this aspect is more important for resonator designs than actuators.

Table 2 gives an order of magnitude for most important elastic and piezoelectric constants summarized from literature [5-7,10,11] and from several manufacturer datasheets. Values recorded from only one reference are marked with a "~" sign.

Figs. 3-5 picture a series of FEM simulations under COMSOL Multiphysicsä performed for different materials with identical geometry and orientation, i.e. 20x20x0.2 mm$^3$ in XY plane. Three PZT and PMN-PT plates are analyzed. Applied voltage

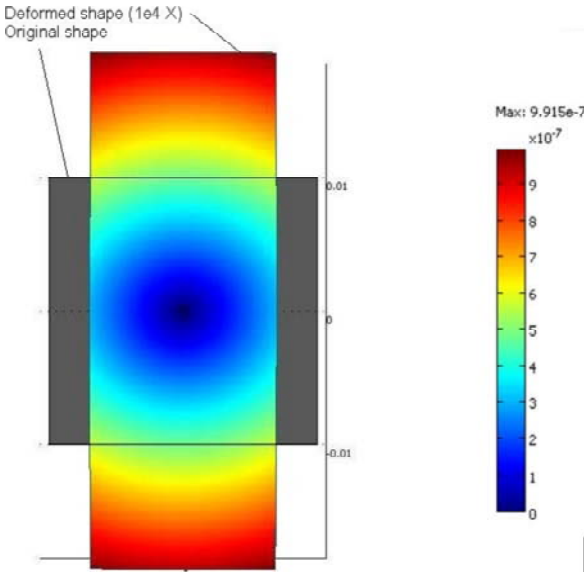


**Fig. 5.** FEM of PMN-29PT plate poled along [011]: original and deformed shape ($10^4$ times). Coefficients taken from [7].

in polarization Z-direction is 10 V ($E_Z$ = –0.5kV/cm). Total displacements are depicted. Deformed shape is magnified 10,000 times for optimal visualization. Largest transverse strain is obtained in Y-direction for the PMN-PT plate poled along [011] plate, as in Fig. 5.

As seen, PMN-PT and PZN-PT (same characteristics as PMN-PT) are around 3 to 5 times more piezoelectric than PZT ceramics. However their compliance is higher, privileging strain to stress. Electromechanical coupling coefficients are very high, usually ranging from 0.8 up to 0.97. Reported density is higher than that of PZT ceramics, of around 8060-8200 kg/m$^3$. Dielectric constants are also higher than that of PZT, for instance $\varepsilon^T_{33}$ can exceed a value of 7500 for certain concentrations.

Manufacturers such as TRS Technologies, JFE Mineral, Morgan Electroceramics, HC Materials,

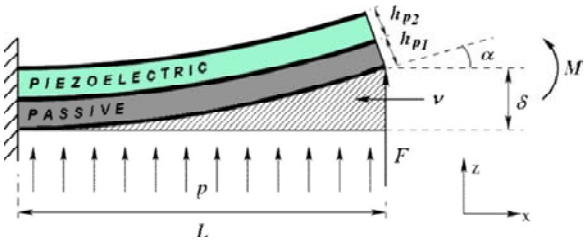


**Fig. 6.** Composite bimorph cantilever.

APC International have started selling custom plates of PMN-PT especially, which is recorded to be more mechanically stable than PZN-PT. We notice that there is a large dispersion in material constants provided by different manufacturers, explainable not only by various material compositions but also by proprietary growing processes. Manufacturers provide limited information about their materials; it is very rare to easily find all necessary material constants. This is a reason why in Section 4 we use the complete sets of matrices investigated by [5,7,10,11] rather than incomplete manufacturer datasheets.

## 3. CONSTITUTIVE EQUATIONS FOR BENDING CANTILEVERS.

In [15] J.G. Smits and W.S. Choi provided an enakemesomorph matrix *E* between the following quantities for a blocked-free beam: beam rotation angle $\alpha$, tip displacement $\delta$, displaced volume $\nu$ and electrical charge *Q* on one side and on the other side, a mechanical moment *M*, an external transverse force *F* (along z-direction, at the end of the beam), a uniform load *p* and an electrical voltage $V_z$ as in Fig. 6.

The constituent equation set applies for heterogeneous bimorphs, (sometimes referred as unimorphs) at thermodynamic equilibrium. Starting from well-known strain-charge coupled equations, the energy density is integrated and summed for the piezoelectric and the passive element. Then the canonical conjugates with the external quantities (voltage, momentum, etc.) are determined by partial derivatives, providing elements for the *E* matrix.

M. Weinberg [16] presented a rather different approach, more related to structural mechanics and dedicated for multilayer beams. Constitutive equation set was extended to include axial tension/compression. Neutral axis is determined, then piezoelectric axial force and torque per unit voltage. Curvature related to different parameters is derived and constitutive coefficients are provided. Even though the deriving method is different than [15], simulations prove identical results.

[17] proposed a modeling analog to that of Smits but for a specific type of duo-bimorph actuators (that allowed both in plane and out of plane displacement). In this paper we eventually adapted the general equations from [17] to derive the transverse free tip displacement $\delta_{z\_free}$ for a beam of length *L* and width *w*:

$$\delta_{z\_free} = \frac{3L^2}{B_1}\left[\frac{d_{31}^{p1}}{s_{11}^{p1}}H_1 + \frac{d_{31}^{p2}}{s_{11}^{p2}}H_2\right]V_z, \tag{1}$$

where *p*1 and *p*2 superscripts refer by convention to the two layers: passive and piezoelectric respectively. $s_{11}^{p1}$ and $s_{11}^{p2}$ are the compliance coefficients at constant electric field and $d_{31}^{p2}$ is the piezoelectric coefficient ($d_{31}^{p1}$ = 0 in our case). Other terms are:

$$H_1 = h_{p1} + h_g - 2\bar{z}, \tag{2}$$

$$H_2 = h_{p2} + h_g + 2\bar{z}, \tag{3}$$

$$\bar{z} = \frac{1}{2}\frac{\left(h_{p1}\left(h_{p1}+h_g\right)/s_{11}^{p1}\right) - \left(h_{p2}\left(h_{p2}+h_g\right)/s_{11}^{p2}\right)}{\left(h_{p1}/s_{11}^{p1}\right)+\left(h_g/s_{11}^{g}\right)+\left(h_{p2}/s_{11}^{p2}\right)}, \tag{4}$$

$$B_1 = \frac{h_{p1}}{s_{11}^{p1}}\left(3h_g^2 + 6h_g\left(h_{p1} - 2\bar{z}\right) + 4\left(h_{p1}^2 - 3\bar{z}h_{p1} + 3\bar{z}^2\right)\right) + \frac{h_{p2}}{s_{11}^{p2}} \times \left(3h_g^2 + 6h_g\left(h_{p2} + 2\bar{z}\right) + 4\left(h_{p2}^2 + 3\bar{z}h_{p2} + 3\bar{z}^2\right)\right) + \frac{h_g}{s_{11}^{g}}\left(h_g^2 + 12\bar{z}^2\right), \tag{5}$$

where $h_{p1}$ and $h_{p2}$ are the thickness of passive and piezoelectric layers respectively while *hg* is the thickness of the interface layer (adhesive). The latter was neglected here for a first approximation.

If an external transverse force $F_z$ is applied at the end of the beam, displacement becomes:

$$\delta_z = \frac{4L^3}{B_1 w}F_z + \frac{3L^2}{B_1}\left[\frac{d_{31}^{p1}}{s_{11}^{p1}}H_1 + \frac{d_{31}^{p2}}{s_{11}^{p2}}H_2\right]V_z. \tag{6}$$

Blocking force $F_{z\_blocking}$ for zero tip displacement is used to provide information related to beam stiffness. For the same $V_z$ voltage and using small displacements approximation we have:

$$F_{z\_blocking} = -\left(B_1 w / 4L^3\right)\delta_{z\_free}. \tag{7}$$

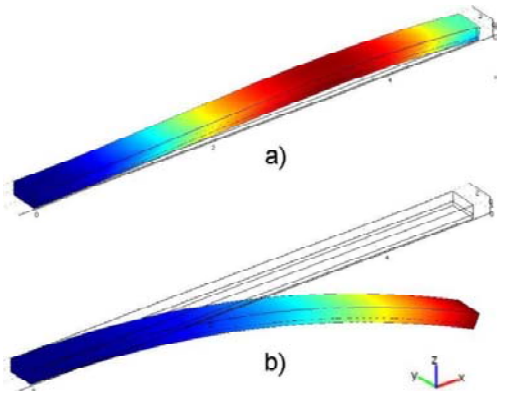


**Fig. 7**. FEM evaluation of: (a) blocking force mode and (b) free tip displacement mode of a 5.0x0.3x0.14 mm$^3$ PZT on Cu actuator submitted to 80 V in the polrization direction (-8.0 kV/cm). Deformed shapes are magnified around 50 times.

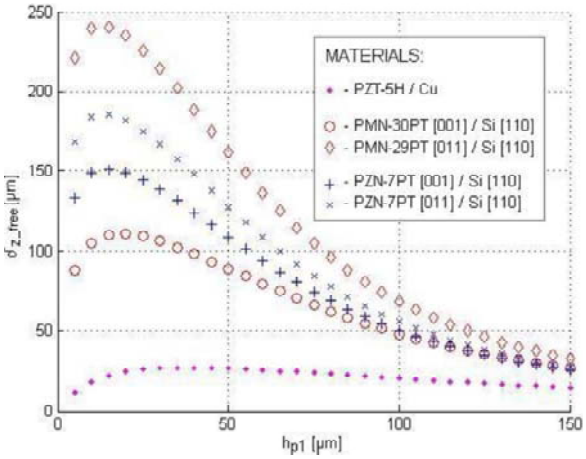


**Fig. 8.** Analytical comparative diagram of free tip displacement with respect to passive layer thickness for different materials. Piezoelectric layer is 0.1 mm thick, length is 5 mm, width is 0.3 mm and applied voltage 80 V.

In depicted formulae the free displacement $\delta_{z\_free}$ varies with the square of the length $L$ while blocking force $F_{z\_blocking}$ varies linearly with the width $w$ and inversely proportional with $L^3$.

## 4. COMPARATIVE RESULTS BETWEEN PZT ON COPPER AND PMN-PT ON SILICON

In this section, analytical expressions (1) and (7) are employed for free end displacement and related blocking force. Alternately, finite elements modeling (FEM) results are provided (Fig. 7).

We consider the stiffness coefficients for copper $s_{11}^{p1}$ =1/110x10$^{-9}$ m$^2$/N (1/110 GPa) and for silicon $s_{11}^{p1}$ =1/170x10$^{-9}$ m$^2$/N. Silicon modulus of 170 GPa corresponds to [110] direction from a {100} wafer. The following five material combinations will be modeled:

· PZT-5H on Copper:
$d_{31}^{p2}$ = -274x10$^{-12}$ m/V; $s_{11}^{p2}$ = 16.5x10$^{-12}$ m$^2$/N;

· PMN-30PT poled along [001] on Silicon [110] X-direction:
$d_{31}^{p2}$ = -921×10$^{-12}$ m/V; $s_{11}^{p2}$ = 52x10$^{-12}$ m$^2$/N; data from [5].

· PMN-29PT poled along [011] on Silicon [110]:
$d_{32}^{p2}$ = -1883×10$^{-12}$ m/V; $s_{22}^{p2}$ = 112×10$^{-12}$ m$^2$/N; data from [7].

· PZN-7PT poled along [001] on Silicon [110]:
$d_{31}^{p2}$ = -1204×10$^{-12}$ m/V; $s_{11}^{p2}$ = 85.9x10$^{-12}$ m$^2$/N; data from [10].

· PZN-7PT poled along [011] on Silicon [110]:
$d_{32}^{p2}$ = -1460×10$^{-12}$ m/V; $s_{22}^{p2}$ = 102x10$^{-12}$ m$^2$/N ; data from [11].

*Note:* PMN-29PT [011] and PZN-7PT [011] actuators are oriented along Y-axis in order to fully benefit from $d_{32}$ coefficient.

We consider an applied voltage of 80 V in the polarization direction, knowing that maximum allowed electric field for PZT varies from 7 to 10 kV/cm. Geometry is $L$ = 5.0 mm by $w$ = 0.3 mm with a fixed piezoelectric layer thickness of $h_{p2}$ =100 µm. Passive layer thickness $h_{p1}$ is considered as variable and its optimum value for the given material pairs is investigated.

As seen from Fig. 8 obtained from calculation of Eq. (1), optimal passive layer thickness for best displacement is 37 µm for PZT-5H on Copper, 19 µm for PMN-30PT [001] on Silicon and 13 µm for PMN-29PT [011] on Silicon. In the case of the PZN-7PT [001] and [011] optimal silicon thickness are 15 µm and 14 µm respectively. Smaller stiffness coefficients of PMN-PT and PZT-PT than PZT favour displacement to blocking force (smaller blocking force gain, Fig. 9), which is an advantage for microactuators and micromanipulators. Maximum ratio of displacement gain is 3.8 for PMN-30PT [001] (actuator along X-direction) and 8.9 in the case of PMN-29PT [011] (actuator along Y-direction).

Figs. 10 and 11 respectively illustrate the analytical calculation of the free displacement and of the blocking force according to the cantilever length. According to one's specific application, the designer should choose the appropriate length that privileges force or displacement. A more general illustration of the trade-off is shown in Fig. 12.

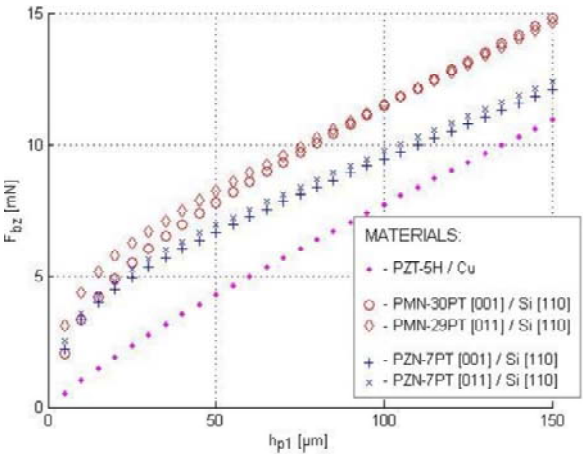


**Fig. 9.** Comparative diagram of blocking force with respect to passive layer thickness for different materials (analytical).

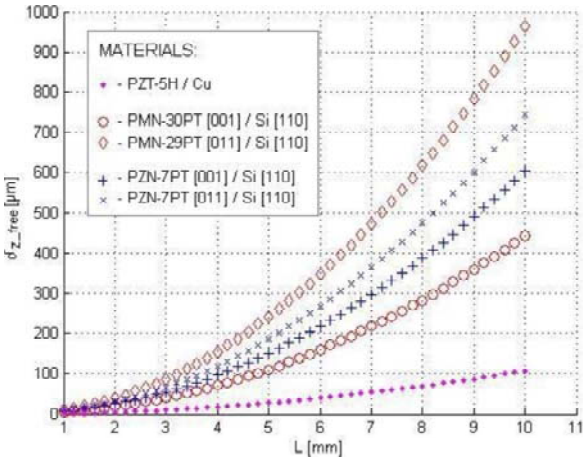


**Fig. 10.** Free tip displacement as a function of length (analytical).

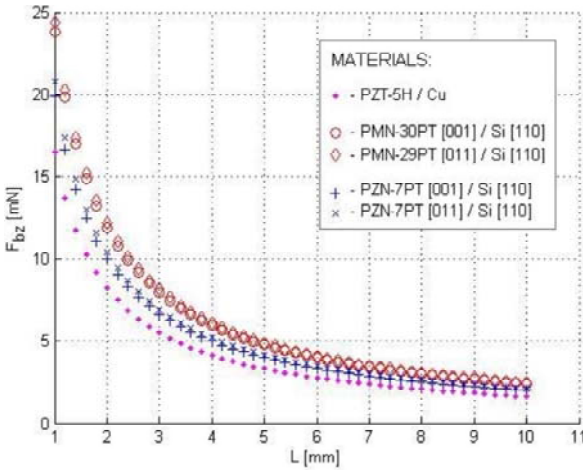


**Fig. 11.** Blocking force dependence on beam length (analytical).

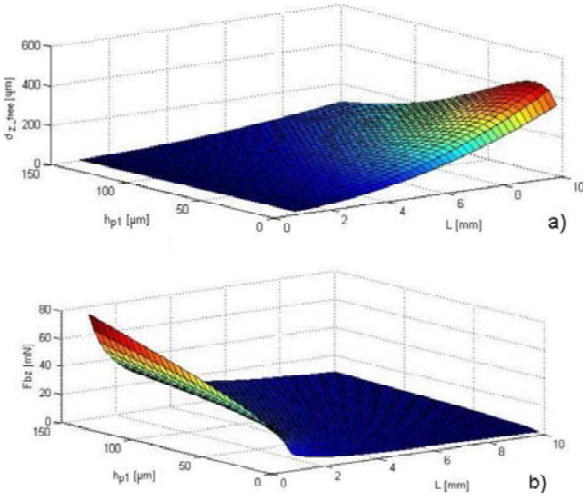


**Fig. 12.** (a) Free tip displacement and (b) blocking force dependence on silicon thickness $h_{p1}$ and beam length $L$. Material is PMN-30PT poled along [001] axis of 0.1 mm thick and 0.3 mm wide.

Anisotropy of silicon Young's modulus makes displacement and blocking force slightly depending on wafer orientation. Fig. 13 shows PMN-30PT curves for different silicon cuts. We considered actuator geometry along [100], [110], and [111] directions, for which related tensile modulus is 130 GPa, 170 GPa, and 189 GPa respectively. A very small improvement is obtained for the orientation [111] for which corresponding Young's modulus is the highest. Figs. 12a and 12b summarize actuating dependence on length $L$ and passive layer thickness $h_{p1}$ for PMN-30PT.

Figs. 14 and 15 depict simulation results performed by FEM analysis considering the same bimorphs than previously. Results show that blocking force obtained with FEM is similar to the analytical ones. However, significant differences in terms of maximum free tip displacement which is lower especially for PMN-PT and PZN-PT occur. The relative difference between FEM and analytical results reach -37%, -69%, -50%, and -58% for PMN-30PT[001], PMN-29PT[011], PZN-7PT[001], and PZN-7PT[011] respectively. For PZT-5H the difference is more acceptable, of around -18%.

Several arguments may explain these differences. First, Smits and Choi [15] as well as Weinberg [16] methods treat in-plane problems where electric field distribution is like that from a plane capacitor. The effect of mechanical strain and stress on electric field is not taken into account. Also, analytical methods don't take into account the electromechanical coupling factor ( $k_{31} = d_{31} / \sqrt{s_{11}^E \varepsilon_{33}^T}$ ) that influences on electrical displacement. For PZT-5H $k_{31}$ equals 0.38 and for [001]-poled single crystals it

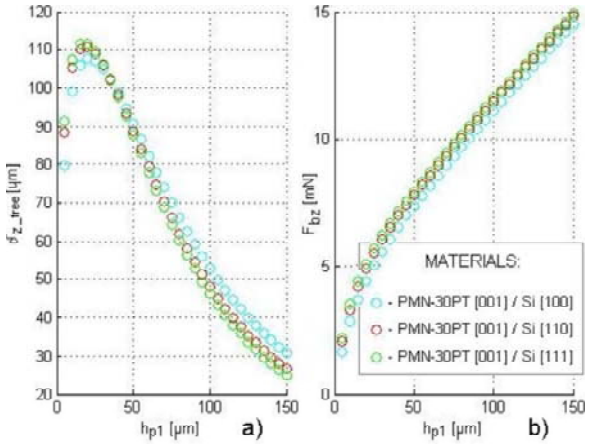


**Fig. 13.** (a) Free tip displacement and (b) blocking force dependence of silicon layer thickness. Traces for PMN-30PT poled along [001] and three silicon directions: [100], [110], and [111].

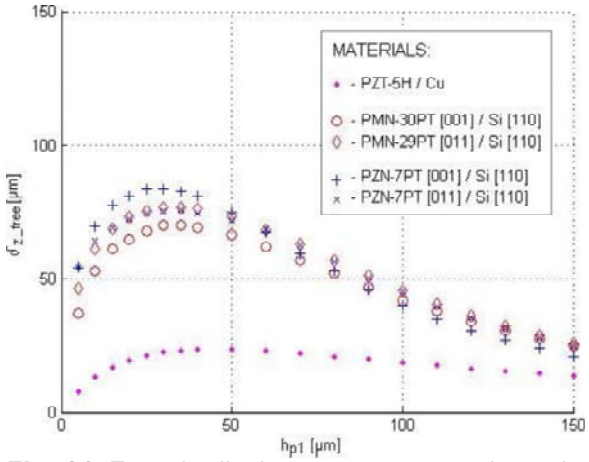


**Fig. 14.** Free tip displacement w.r.t passive substrate thickness (FEM analysis). Length is 5 mm, width is 0.3 mm and piezoelectric layer thickness is 0.1 mm.

larger: 0.49 and 0.58 for PMN-30PT and PZN-7PT respectively. For materials poled along [011], homologue $k_{32}$ factors are 0.94 and 0.86 for PMN-29PT and PZN-7PT. There is a correlation between these coupling factor values and differences noticed and depicted the paragraph above. Obviously, working expressions (1) and (7) miss out those coupling coefficients that over-estimate the electrical field and increase the actual mechanical stiffness. Finally, for the analytical methods, the neutral fiber position is fixed. However, in fact, for composite bimorph design and especially for high coupling factor materials, the neutral fiber position is varying according to the applied voltage. Hence, the immediate consequence is the reduction of the free tip displacement.

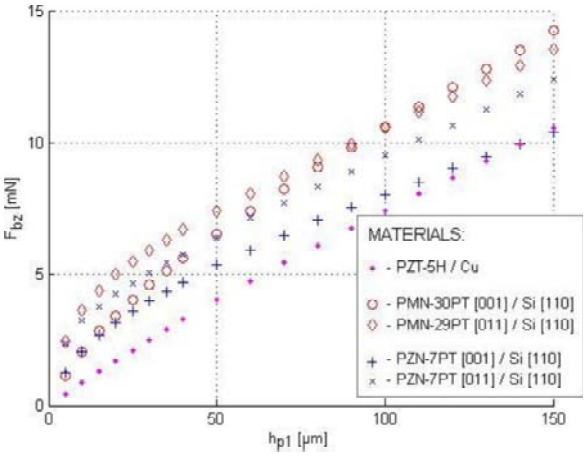


**Fig. 15.** Blocking force w.r.t passive substrate thickness (FEM analysis). Same dimensions as in figure 14.

Notice that in our case, the utilized width (0.3 mm) is quite comparable to total thickness (0.11…0.25 mm). The analysis of such a case should be done with 3D rather than actual 2D boundary conditions. This is why the differences between analytical and FEM methods are primarily explained by inherent simplifications of analytical model. While FEM method treats the coupling problem more "rigorously", in 3D, the lateral deformations are not taken into account by analytical methods. Hence, there exists a curvature in the YZ cross-section of the cantilever, due to interfacial stress between piezoelectric of the silicon layers, that analytical methods do not take into account.

## 5. FINAL REMARKS

Compared to PZT ceramics, PMN-PT and PZN-PT single crystal materials are around three to five times more piezoelectric, making actuation range increasing substantially, as seen in Section IV. Comparative results were related to a similar geometry, dimensions and same applied voltage. Maximum applicable voltage however differs. As an average, manufacturers usually restrict maximum bipolar working fields for soft PZTs to ±8 kV/cm while PMN-PT may be driven between around –2 kV/cm and +25 kV/cm (TRS Technologies). This means that PMN-PT may be driven up to 68% more voltage than PZT, allowing a theoretical increase of the actuating range. However these values must be considered informative, as we did not take into account material nonlinearities (e.g. hysteresis) or the quadratic electrostrictive effect that comes into place

at high voltages. Also, significant differences were noticed between finite element results and analytical ones. As discussed in section-IV, the latter model should be ameliorated by taking into account the very high coupling factor of these materials.

As drawbacks for single crystal high piezoelectric coefficient PMN-PT and PZN-PT, their compliance coefficients are higher, implying some limitations in blocking force (smaller increase than that of free displacement). For manufacturing, tensile stresses should be avoided and compressive loads limited to a couple MPa. However these aspects are impediments more likely for piezoelectric stack actuators rather than described composite bimorphs intended for fragile micro-objects manipulation. Other cautions to be taken into account with single crystals refer to a more mechanically fragile structure than PZT and to a lower coercitive field of around 2.5 to 4.5 kV/cm that limits full bipolar driving capabilities. Some temperature dependence is discussed in [12]. Curie temperature is lower for these single crystals than PZT ceramics, ranging around 150 °C. Finally, their working temperature is limited by some manufacturers below 80-85 °C.

## 6. CONCLUSION

This paper has presented a comparative study of performances of PMN-PT and PZN-PT single crystals and PZT materials based piezocantilever actuators. The analyzed performances concern the blocking force and the tip displacement, and for this purpose both analytical constitutive expressions and FEM simulations were employed. A significant difference between the two types of simulation was noticed and explained, FEM method is more reliable for high coupling factor materials. PMN-PT and PZN-PT are three to five times more piezoelectric than PZT. On the other hand, blocking forces for these single crystal materials are comparable to that of PZT. As seen, relating on specific application and geometry restrictions, there are different trade-offs privileging displacement range or blocking force. The results and discussions show that PMN-PT and PZN-PT materials are very attractive for designing silicon integrated microactuators, providing high range of displacement and high resolution.

## REFERENCES

[1] M. Sitti, D. Campolo, J. Yan, R.S. Fearing, T. Su, D. Taylor and T. Sands, In: *Development of PZT and PZN-PT Based Unimorph Actuators for Micromechanical Flapping Mechanisms* (IEEE Int. Conf. Robotics and Automation, Seoul Korea, 2001), p. 3839.

[2] B. Ko and B. H. Tongue // *Smart Mater. Struct.* **15** (2006) 1912.

[3] A.J. Moulson and J.M. Herbert, *Electroceramics: Materials, Properties, Applications 2nd Edition* (John Wiley and Sons, 2003).

[4] S. Muensit, P. Sukwisut, P. Khanemkeaw and S.B. Lang // *Appl .Phys. A*. **92** (2008) 659.

[5] R. Zhang, W. Jiang, B. Jiang and W. Cao // *AIP Conf. Proc*. **626** (2002) 188.

[6] H. Cao, V. H. Schmidt, R. Zhang and W. Cao // *J. of Appl. Phys.* **96** (2004) 549.

[7] F. Wang, L. Luo, D. Zhou, X. Zhao and H. Luo // *Appl. Phys. Lett.* **90** (2007) 212903.

[8] A. M. Moisin, A. I. Dumitru, I. Pasuk and G. Stoian // *J. of Optoel. and Adv. Mat.* **8** (2006) 555.

[9] P. Kumar, S. Sharma, O.P. Thakur, C. Prakash and T.C. Goel // *Ceramics International* **30** (2004) 585.

[10] R. Zhang, B. Jiang and W. Cao // *J. of Mat. Sci. Lett.* **21** (2002) 1877.

[11] R. Zhang, B. Jiang and W. Cao // *Applied Phys. Lett.* **89** (2006) 242908.

[12] L. Lebrun, G. Sebald, B. Guiffard, C. Richard, D. Guyomar and E. Pleska // *Ultrasonics* **42** (2004) 501.

[13] Y. M. Kim, S. H. Lee, H. Y. Lee, and Y. R. Roh, In: *Measurement of all the material* properties of PMN-PT syngle crystals grown by the Solid-State-Crystal-Growth (SSCG) *method* (2003 IEEE Ultrasonics Symp., 2003) p. 1987.

[14] A. Hall, M. Allahverdi, E.K. Akdogan and A. Safari // *Journal of Electroceramics* **15** (2005) 143.

[15] J.G. Smits and W.S. Choi, In: *The constituent equations of piezoelectric heterogeneous bimorphs* (IEEE Ultrasonic Symposium, 1990), p. 1275.

[16] M.S. Weinberg // *ASME/IEEE Journal of MEMS* **8** (1999) 71.

[17] P. De Lit, J. Agnus and N. Chaillet, In: *Proc. of Int. Symp. on Assembly and Task Planning* (France-Comte Univ., ISAPT, 2003) p. 1.